Aalborg Universitet

AALBORG UNIVERSITY
DENMARK

Improved rotor flux observer for sensorless control of PMSM with adaptive harmonic elimination and phase compensation

Xu, Wei; Wang, Lei; Liu, Yi; Blaabjerg, Frede

Published in:
CES Transactions on Electrical Machines and Systems

DOI (link to publication from Publisher):
10.30941/CESTEMS.2019.00021

Publication date:
2019

Document Version
Publisher's PDF, also known as Version of record

Link to publication from Aalborg University

Citation for published version (APA):
Xu, W., Wang, L., Liu, Y., & Blaabjerg, F. (2019). Improved rotor flux observer for sensorless control of PMSM with adaptive harmonic elimination and phase compensation. *CES Transactions on Electrical Machines and Systems* , *3*(2), 151 - 159. https://doi.org/10.30941/CESTEMS.2019.00021

General rights
Copyright and moral rights for the publications made accessible in the public portal are retained by the authors and/or other copyright owners and it is a condition of accessing publications that users recognise and abide by the legal requirements associated with these rights.

- Users may download and print one copy of any publication from the public portal for the purpose of private study or research.
- You may not further distribute the material or use it for any profit-making activity or commercial gain
- You may freely distribute the URL identifying the publication in the public portal -

Take down policy
If you believe that this document breaches copyright please contact us at vbn@aub.aau.dk providing details, and we will remove access to the work immediately and investigate your claim.

Improved Rotor Flux Observer for Sensorless Control of PMSM with Adaptive Harmonic Elimination and Phase Compensation

Wei Xu, *Senior Member, IEEE*, Lei Wang, Yi Liu., *Member, IEEE,* Frede Blaabjerg, *Fellow*, *IEEE*
(Invited)

***Abstract*—In this paper, a sensorless control strategy of a permanent magnet synchronous machine (PMSM) based on an improved rotor flux observer (IFO) is proposed. Due to the unknown integral initial value and the high harmonics caused by current sampling and inverter nonlinearities, the flux linkage estimated by traditional rotor flux observer may be inaccurate. In order to address these issues, a self-adaptive band-pass filter (SABPF) is designed to eliminate the DC component and high-frequency harmonics of the estimated equivalent rotor flux linkage. Furthermore, in order to avoid that the design of PI parameter is influenced by the amplitude of equivalent rotor flux linkage, an improved phase-locked loop (IPLL) is employed to obtain the rotor speed and to normalize the estimated equivalent rotor flux linkage. In addition, angle shift caused by an SABPF is compensated to improve the accuracy of the estimated flux linkage angle. Besides, the parameter robustness of this method is analyzed in detail. Finally, simulation and experimental results demonstrate the effectiveness and parameter robustness of the proposed method.**

***Index Terms*—Improved phase-locked loop (IPLL), sensorless control, improved flux observer (IFO), self-adaptive band-pass filter (SABPF).**

I. Introduction

PERMANENT magnet synchronous motors (PMSM) are widely used in the industrial field owing to its high power density, high reliability. Further the rotor position and rotor speed are essential in the field-oriented control (FOC). Generally, encoders or sensors are used to obtain the position. However, the installation of encoder may increase the cost, stability and complexity of PMSM drive system. Thus, sensorless control is in ascendant of PMSM drive system.

Currently, there are several sensorless control algorithms of PMSM drive systems, including direct calculation method [1], flux observer [2], extend back-electromotive force estimator [3], model reference adaptive system (MRAS) [4], sliding mode observer (SMO) [5-6], extended Kalman filter (EKF) [7], Luenberger observer [8], high-frequency signal injection (HFI) [9], artificial intelligence-based estimator [10], etc. The direct calculation method calculates the back-electromotive force directly by stator voltage equation and obtains the estimated rotor position by arctangent. This method is very dependent on the parameters, and the estimated rotor position is not regulated. EMF method rearranges the mathematical model of PMSM to obtain the EMF, which is used to estimate the rotor speed and position. MRAS method constructs an adjustable model by mathematical model, and designs adaptive rate to regulate the adjustable model to ensure to outputs of two model are consistent. Therefore, MRAS can obtain the rotor speed and position by adjustable model. SMO estimates the rotor speed and position by constructing Lyapunov function and sliding surface. HFI is only suitable for interior permanent magnet synchronous machine at low speed. In this paper, a sensorless control algorithm based on an improved flux observer is proposed.

Based on the mathematical model of PMSM, rotor position can be obtained by alpha-beta axis flux linkage. Generally, the rotor flux linkage is integrated by Equivalent back-electromotive force (EMF), which is obtained by stator voltage and stator current. However, the DC component and high-frequency harmonics might be generated in the current sampling and the nonlinearity of the converter. Furthermore, stator resistance may vary with the temperature while motor running, and the stator inductance may vary with the load. Therefore, due to the unknown integral initial value, the high-frequency harmonics and mismatch of parameters, the conventional flux observer is unable to estimate the rotor speed and position accurately. Currently, some methods are proposed to solve the problem. Such as disturbance observer and initial flux condition estimator [11]. However, the proposed methods can't guarantee the effectiveness. As for LPF [12], the pure integral is replaced by an LPF, and this method can eliminate the DC component, but the phase shift might be generated in

Manuscript was submitted for review on 06, May, 2019
This work has been partly supported by National Natural Science Foundation of China (NSFC 51877093,51707079,and 51807075) , National Key Research and Development Program of China (Project ID: YS2018YFGH000200), and Fundamental Research Funds for the Central Universities (2019kfyXMBZ031)
W, Xu, L, Wang, and Y, Liu (Corresponding Author) are with the State Key Laboratory of Advanced Electromagnetic Engineering and Technology, School of Electrical and Electronic Engineering, Huazhong University of Science and Technology, Wuhan, 430074, China. (E-mails: weixu@hust.edu.cn; wayfe@foxmail.com; liuyi82@hust.edu.cn)
F. Blaabjerg is with the Department of Energy Technology, Aalborg University, Aalborg 9220, Denmark (e-mail: fbl@et.aau.dk).
Digital Object Identifier 10.30941/CESTEMS.2019.00021

estimated equivalent rotor flux linkage. Thus, the proposed method is also unable to obtain the rotor speed and position accurately. Meanwhile, a SOIFO-FLL method is proposed in [13] where the proposed method can reduce but not eliminate the DC component. Furthermore, a second-order SOIFO-FLL is proposed in [14], and this method can eliminate the DC component and high-frequency harmonic. However, the calculation process of the proposed method is very complex, and the practicality is unable to be guaranteed.

In this paper, a useful and simple method is proposed to solve about the mentioned problem. Firstly, a self-adaptive band-pass filter (SABPF) is used to eliminate DC component and high-frequency harmonics. Then, an improved phase-locked loop (IPLL) is used to obtain the rotor speed and uncompensated position. Next, the estimated rotor position is compensated. Furthermore, analysis of parameter robustness is provided. Ultimately, the accuracy and feasibility are verified by and experimental results.

II. Conventional Flux Observer

Based on the mathematical model of PMSM, rotor position can be obtained by alpha-beta axis flux linkage which is generally integrated by EMF.

A. Flux Observer for Sensorless Control

For interior permanent magnet synchronous motor (IPM), the model can be described as:

$$\begin{bmatrix} u_\alpha \\ u_\beta \end{bmatrix} = \begin{bmatrix} R_s + pL_\alpha & pL_\beta \\ pL_\alpha & R_s + pL_\beta \end{bmatrix} \begin{bmatrix} i_\alpha \\ i_\beta \end{bmatrix} + \omega_r \lambda_m \begin{bmatrix} -sin\theta_r \\ cos\theta_r \end{bmatrix} \tag{1}$$

where u_α and u_β are the α-axis and β-axis stator voltages, i_α and i_β are the α-axis and β-axis stator currents, R_s is the stator resistance, p is the differential operator, ω_r is the rotor speed, θ_r is the rotor position, λ_m is the rotor flux linkage. L_α, $L_{\alpha\beta}$ and L_β are temporary variables, whose values are:

$$\begin{bmatrix} L_\alpha \\ L_\beta \\ L_{\alpha\beta} \end{bmatrix} = \frac{1}{2} \begin{bmatrix} L_d + L_q + (L_d - L_q)\, cos2\theta \\ L_d + L_q - (L_d - L_q)\, cos2\theta \\ (L_d - L_q)\, sin2\theta \end{bmatrix} \tag{2}$$

From (1), it can be obtained that:

$$\begin{bmatrix} u_\alpha \\ u_\beta \end{bmatrix} = \begin{bmatrix} R_s + pL_q & 0 \\ 0 & R_s + pL_q \end{bmatrix} \begin{bmatrix} i_\alpha \\ i_\beta \end{bmatrix} + p \begin{bmatrix} \lambda'_\alpha \\ \lambda'_\beta \end{bmatrix} \tag{3}$$

where λ'_α and λ'_β are the α-axis and β-axis equivalent rotor flux linkage. And the α-β-axis equivalent back-electromotive force e'_α and e'_β can be expressed as

$$\begin{bmatrix} e'_\alpha \\ e'_\beta \end{bmatrix} = p \begin{bmatrix} \lambda'_\alpha \\ \lambda'_\beta \end{bmatrix} = \omega_r [\,(L_d - L_q)\, i_d + \lambda_m] \begin{bmatrix} -sin\theta_r \\ cos\theta_r \end{bmatrix} \tag{4}$$

where L_d and L_q are the d-axis and q-axis stator inductance, i_d is the d-axis stator current. Thus, we could get the equivalent rotor flux linkage in the α-β reference frame by integrating equation (3) as the following:

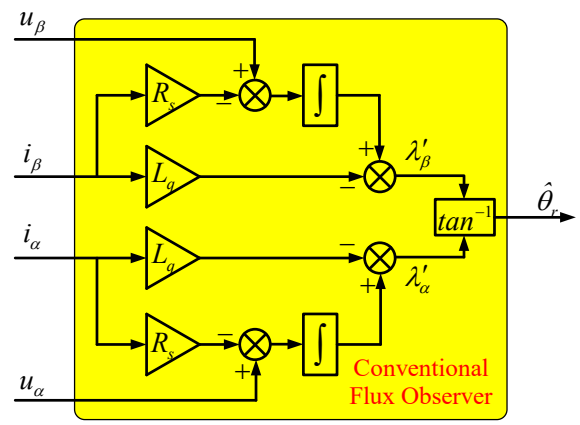

Fig. 1. Structure diagram of conventional flux observer in a PMSM.

$$\begin{bmatrix} \lambda'_\alpha \\ \lambda'_\beta \end{bmatrix} = -L_q \begin{bmatrix} i_\alpha \\ i_\beta \end{bmatrix} + \int \begin{bmatrix} u_\alpha - Ri_\alpha \\ u_\beta - Ri_\beta \end{bmatrix} \tag{5}$$

Therefore, the estimated rotor position $\hat{\theta}_r$ can be obtained as:

$$\hat{\theta}_r = tan^{-1}\left(\lambda'_\beta / \lambda'_\alpha\right) \tag{6}$$

And the Structure diagram of conventional flux observer in a PMSM is shown in Fig. 1.

B. Analysis of Conventional Flux Observer

From equation (5), the conventional flux observer has a pure integral structure. And the ideal estimated flux linkage can be obtained as the following:

$$\begin{bmatrix} \hat{\lambda}'_\alpha \\ \hat{\lambda}'_\beta \end{bmatrix} = -L_q \begin{bmatrix} i_\alpha \\ i_\beta \end{bmatrix} + \int \begin{bmatrix} u_\alpha - R_s i_\alpha \\ u_\beta - R_s i_\beta \end{bmatrix} = k \begin{bmatrix} cos\theta_r \\ sin\theta_r \end{bmatrix} \tag{7}$$

However, the DC component may be generated in the sampling of the stator current while the motor is running. Therefore, the estimated flux linkage may be realized due to the pure integral block. Furthermore, high-frequency harmonics may be generated in stator voltage because of the nonlinearities of the inverter. Thus, the actual estimated flux linkage might be:

$$\begin{bmatrix} \hat{\lambda}'_\alpha \\ \hat{\lambda}'_\beta \end{bmatrix} = k \begin{bmatrix} cos\theta_r \\ sin\theta_r \end{bmatrix} + \begin{bmatrix} a \\ b \end{bmatrix} \tag{8}$$

where a and b are DC component and high-frequency harmonics of α-axis and β-axis estimated stator flux linkage. In this case, the actual rotor position is not equal to the estimated rotor position:

$$\theta_r = tan^{-1} \frac{ksin\theta_r}{kcos\theta_r} \neq \hat{\theta}_r = tan^{-1} \frac{ksin\theta_r + b}{kcos\theta_r + a} \tag{9}$$

Therefore, the conventional flux observer is unable to estimate rotor speed and position accurately.

III. Improved Flux Linkage Observer

An IFO is proposed in this section to obtain a more accurate rotor position. The IFO uses the SABPF to eliminate the DC component and high harmonics. Also, an IPLL is used to obtain the rotor position instead of using a division. Meanwhile, phase

error caused by SABPF is compensated by phase compensation block. The structure diagram is shown in Fig. 2.

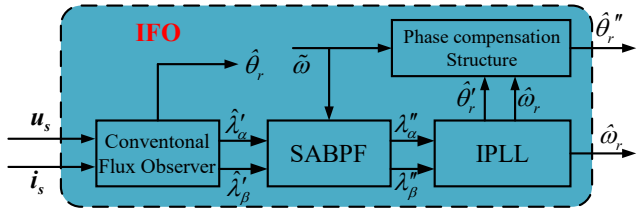

Fig. 2. Structure diagram of improved flux observer.

A. Self-Adaptive Band-Pass Filter

In order to avoid a pure integrator to amplify the DC component, and considering high-frequency harmonic caused by the nonlinearities of the inverter, an SABPF is used to obtain the fundamental component of the estimated stator flux linkage. Fig. 3 shows the structure diagram of SABPF.

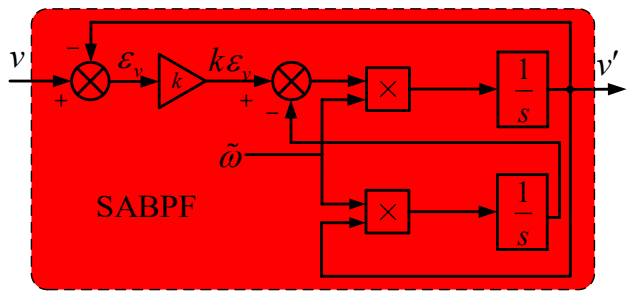

Fig. 3. Structure diagram of self-adaptive band-pass filter.

The transfer function can be described as:

$$G(s)=\frac{v'}{v}=\frac{k\tilde{\omega}s}{s^2+k\tilde{\omega}s+\hat{\omega}_r^{\,2}} \tag{10}$$

where v is the input of the SABPF, v' is the output of the SABPF, k is quality factor, $\tilde{\omega}$ is self-adaptive resonance angular frequency. And the amplitude-frequency characteristic is given as following:

$$|G|=\frac{k\tilde{\omega}\hat{\omega}_r}{\sqrt{(k\tilde{\omega}\hat{\omega}_r)^2+(\hat{\omega}_r^2-\tilde{\omega}^2)^2}} \tag{11}$$

$$\angle G=tan^{-1}\frac{\hat{\omega}_r^2-\tilde{\omega}^2}{k\tilde{\omega}\hat{\omega}_r} \tag{12}$$

From equation (11), the amplitude of SABPF might be decreased where a self-adaptive resonance angular frequency is not equal to the estimated rotor angular frequency. Actually, the flux observer estimates the rotor position instead of flux linkage. Hence, there is no need to consider the decrease of amplitude. However, the phase shift may generate due to the mismatch of $\tilde{\omega}$ .But an angle error might be obtained by equation (12). And the bandwidth and responding speed are decided by the quality factor k. In general, for convenient calculation, $k=\sqrt{2}$.

B. Improved Phase-Locked Loop

In a conventional flux observer, we can only obtain the rotor position by equation (6). However, the rotor speed is also needed in motor control. The rotor speed is generated by differentiation, high-frequency harmonics may be generated in the estimated equivalent rotor speed. Assuming that the output of SABPF is:

$$\begin{bmatrix}\lambda''_\alpha\\ \lambda''_\beta\end{bmatrix}=\frac{k\tilde{\omega}s}{s^2+k\tilde{\omega}s+\hat{\omega}_r^{\,2}}\begin{bmatrix}\hat{\lambda}'_\alpha\\ \hat{\lambda}'_\beta\end{bmatrix}=|G|\lambda_m\begin{bmatrix}cos\theta'_r\\ sin\theta'_r\end{bmatrix} \tag{13}$$

In the conventional PLL, the amplitude of flux linkage has an impact on the design of PI parameters. Therefore, an IPLL is used to obtain the estimated rotor position and speed where the structure diagram of IPLL is shown in Fig. 4.

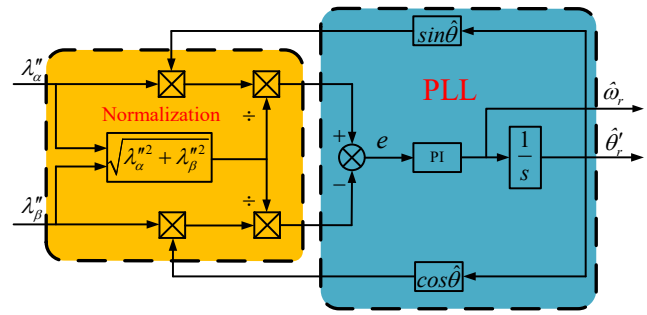

Fig. 4. Structure diagram of improved phase-locked loop.

In order to avoid that the design of PI parameter is influenced by the amplitude of the equivalent rotor flux linkage, the equivalent rotor flux linkage need to be normalized. Furthermore, when the IPLL works nearby steady state [15], it can be linearized as shown in Fig. 5.

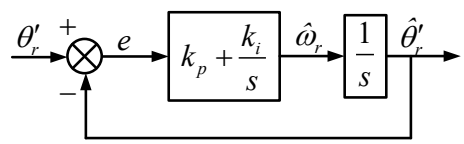

Fig. 5. Structure diagram of improved phase-locked loop with linearization.

The error e can be described as:

$$e=sin\theta'cos\hat{\theta}'-cos\theta'sin\hat{\theta}'\approx\Delta\theta' \tag{14}$$

Further the transfer function can be described as:

$$G_{PLL}(s)=\frac{k_ps+k_i}{s^2+k_ps+k_i} \tag{15}$$

Therefore, the parameters of PI controller can be designed by setting up the settling time t_s and damping coefficient ξ .

$$\begin{cases}t_s=9.2/k_p\ (\pm 2\%)\\ \xi=k_p/2\sqrt{k_i}\end{cases} \tag{16}$$

C. Phase Compensation

From equation (12), phase shift may generate due to the mismatch of self-adaptive resonant angular frequency and estimated rotor angular frequency. Therefore, the phase shift can be compensated by equation (17), and we can obtain the estimated rotor position $\hat{\theta}''_r$ as the following:

$$\hat{\theta}''_r=\hat{\theta}'_r-tan^{-1}\frac{\hat{\omega}_r^2-\tilde{\omega}^2}{k\tilde{\omega}\hat{\omega}_r} \tag{17}$$

D. Analysis of Parameter Robustness

Generally, the parameter of PMSM is mutative when the motor is running. Therefore, it is important to analyze the parameter robustness of proposed method.

In general, stator resistance R_s varies with the motor temperature while the motor operation. Supposed that actual stator resistance is R_s' ,and ΔR_s is the variable value of the stator resistance.

$$R_s' = R_s + \Delta R_s \tag{18}$$

Supposed that the *α-β*-axis stator voltages are:

$$\begin{bmatrix} u_a \\ u_\beta \end{bmatrix} = u_s \begin{bmatrix} sin\left(\omega_r t + \theta_u\right) \\ cos\left(\omega_r t + \theta_u\right) \end{bmatrix} \tag{19}$$

where θ_u is the phase of stator voltage. And the *α-β*-axis stator currents are:

$$\begin{bmatrix} i_\alpha \\ i_\beta \end{bmatrix} = i_s \begin{bmatrix} sin\left(\omega_r t + \theta_i\right) \\ cos\left(\omega_r t + \theta_i\right) \end{bmatrix} \tag{20}$$

where θ_i is the phase of stator current. Therefore, the estimated flux linkage can be derived as :

$$\begin{bmatrix} \hat{\lambda}_\alpha' \\ \hat{\lambda}_\beta' \end{bmatrix} = -L_q \begin{bmatrix} i_\alpha \\ i_\beta \end{bmatrix} + \int m \begin{bmatrix} sin\left(\omega_r t + \phi_R\right) \\ cos\left(\omega_r t + \phi_R\right) \end{bmatrix} dt \tag{21}$$

where *m* and ϕ_R are constant values, and they can be expressed as

$$m = \sqrt{u_s^2 + R_s'^2 i_s^2 - 2R_s' i_s u_s \, cos\left(\theta_u - \theta_i\right)} \tag{22}$$

$$\phi_R = tan^{-1} \frac{u_s \, sin\,\theta_u - R_s \, i_s \, sin\,\theta_i}{u_s \, cos\,\theta_u - R_s \, i_s \, cos\,\theta_i} \tag{23}$$

Considering that $u_s \gg R_s i_s$, equation (21) can be simplified to：

$$\begin{bmatrix} \hat{\lambda}_\alpha' \\ \hat{\lambda}_\beta' \end{bmatrix} \approx -L_q \begin{bmatrix} i_\alpha \\ i_\beta \end{bmatrix} + \int u_s \begin{bmatrix} sin\left(\omega_r t + \phi_R'\right) \\ cos\left(\omega_r t + \phi_R'\right) \end{bmatrix} dt \tag{24}$$

$$\phi_R' \approx tan^{-1}\,\theta_u \tag{25}$$

Therefore, a change of R_s has almost no impact on the estimated flux linkage. Meanwhile, L_q varies with the load torque. Supposing that actual *q-axis* stator inductance is L_q' , and can be expressed as

$$L_q' = L_q + \Delta L_q \tag{26}$$

where ΔL_q is the variable value of the *q-axis* stator inductance. The estimated flux linkages can be expressed as

$$\begin{bmatrix} \hat{\lambda}_\alpha' \\ \hat{\lambda}_\beta' \end{bmatrix} = -\left(L_q + \Delta L_q\right) \begin{bmatrix} i_\alpha \\ i_\beta \end{bmatrix} + \int u_s \begin{bmatrix} sin\left(\omega_r t + \theta_\lambda\right) \\ cos\left(\omega_r t + \theta_\lambda\right) \end{bmatrix} dt \tag{27}$$

where $\theta_\lambda = \left(\theta_u + \theta_i\right)/2 + \phi'$, rearranging (27) to become

$$\begin{aligned} \begin{bmatrix} \hat{\lambda}_\alpha' \\ \hat{\lambda}_\beta' \end{bmatrix} &= -L_q' i_s \begin{bmatrix} sin\left(\omega_r t + \theta_i\right) \\ cos\left(\omega_r t + \theta_i\right) \end{bmatrix} + \frac{u_s}{\omega_r} \begin{bmatrix} cos\left(\omega_r t + \theta_i\right) \\ -sin\left(\omega_r t + \theta_i\right) \end{bmatrix} \\ &= n \begin{bmatrix} cos\left(\omega_r t + \phi_L\right) \\ -sin\left(\omega_r t + \phi_L\right) \end{bmatrix} \end{aligned} \tag{28}$$

where *n* and ϕ_L are constant values, and they can be expressed as

$$n = \sqrt{\frac{u_s^2}{\omega_r^2} + L_q^2 i_s^2 + 2L_q i_s \frac{u_s}{\omega_r} sin\left(\theta_i - \theta_\lambda\right)} \tag{29}$$

$$\phi_L = tan^{-1} \frac{L_q' i_s \omega_r \, cos\,\theta_i + u_s \, sin\,\theta_\lambda}{-L_q' i_s \omega_r \, sin\,\theta_i + u_s \, cos\,\theta_\lambda} \tag{30}$$

Considering that $u_s \gg L_q i_s \omega_r$, the equation (28) can be simplified to：

$$\begin{bmatrix} \hat{\lambda}_\alpha' \\ \hat{\lambda}_\beta' \end{bmatrix} \approx \frac{u_s}{\omega_r} \begin{bmatrix} cos\left(\omega_r t + \phi_\lambda'\right) \\ -sin\left(\omega_r t + \phi_\lambda'\right) \end{bmatrix} \tag{31}$$

where $\theta_\lambda' \approx \theta_\lambda$. Therefore, change of L_q seldom exerts the influence on the estimated flux linkage. Furthermore, L_d and λ_m are not used during the observation.

IV. Simulation And Experimental Results

The block diagram of the sensorless control based on the IFO strategy is shown in Fig. 6. The FOC scheme is used as the basic control scheme. Firstly, the sampled current and voltage are executed Clarke transformation to obtain the *α-β* axis

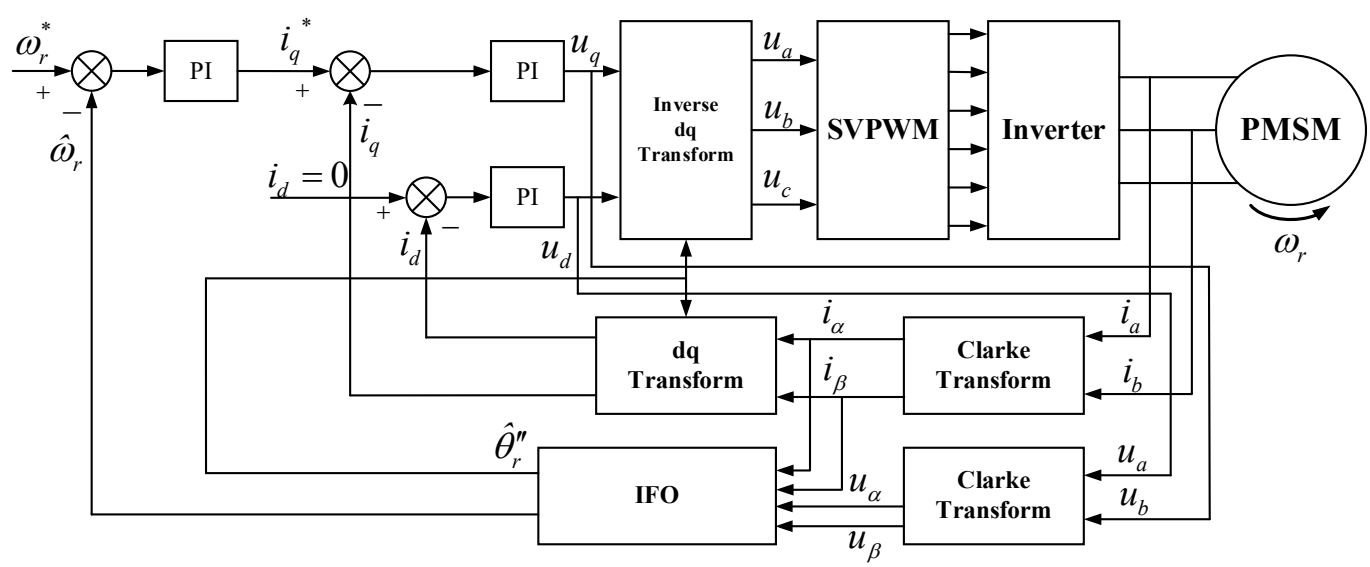

Fig. 6. Structure diagram of sensorless control strategy based on improved flux observer.

current and voltage. Then, the estimated rotor speed and position are provided by the proposed method. Meanwhile, the estimated rotor speed is fed back to the speed loop, and the estimated rotor position is used for executing dq transformation and inverse dq transformation. Furthermore, Table I shows the parameters of PMSM.

TABLE I
PARAMETERS OF PMSM

Symbol	Quantity	Value and Unit
P_n	Rated power	3 kW
I_N	Rated current	6.8 A
n_N	Rated speed	1200 rpm
p_n	Number of pole pairs	3
λ_m	Flux linkage	0.35 Wb
R_s	Stator resistance	1.14 Ω
L_d	d-axis stator inductance	1.19 mH
L_q	q-axis stator inductance	4.73 mH
J	Coefficient of friction	3.78*10^-4 kg*m^2

A. Simulation Results

Fig. 7 shows the simulation results of the conventional flux observer, IFO (before compensation), IFO (after compensation) at 200 r/min with no load. Fig. 7 (a) shows the estimated rotor position and position error of the conventional flux observer. It is obvious that the conventional flux observer is unable to estimate the rotor position accurately. Fig. 7 (b) shows the estimated angle and angle error of the proposed IFO (before compensation). In this figure, the frequency of the estimated rotor position is equal to the actual rotor position. Therefore, the rotor speed estimated by IFO is accurate. However, due to the mismatch of the self-adaptive resonant angular frequency and estimated rotor angular frequency, there exist an angle error (about 1.22 rad) between estimated rotor position and actual rotor position. Fig. 7 (c) presents the estimated rotor position and position error of IFO (after compensation). As it can be seen, the angle error is decreased to less than 0.01 rad after the phase compensation, which guarantees the accuracy of the rotor position estimated by the proposed method at low speed.

Fig. 8 presents the simulation results of the three methods at 900 r/min with no load. Fig. 8 (a) shows the estimated rotor position and position error of conventional flux observer. Fig. 8 (b) shows the estimated angle and angle error of proposed IFO (before compensation). Fig. 8 (c) presents the estimated rotor position and position error of IFO (after compensation). As it can be seen, the conventional flux observer is still unable to estimate the rotor speed and position accurately while the IFO can accurately obtain the rotor speed regardless of phase

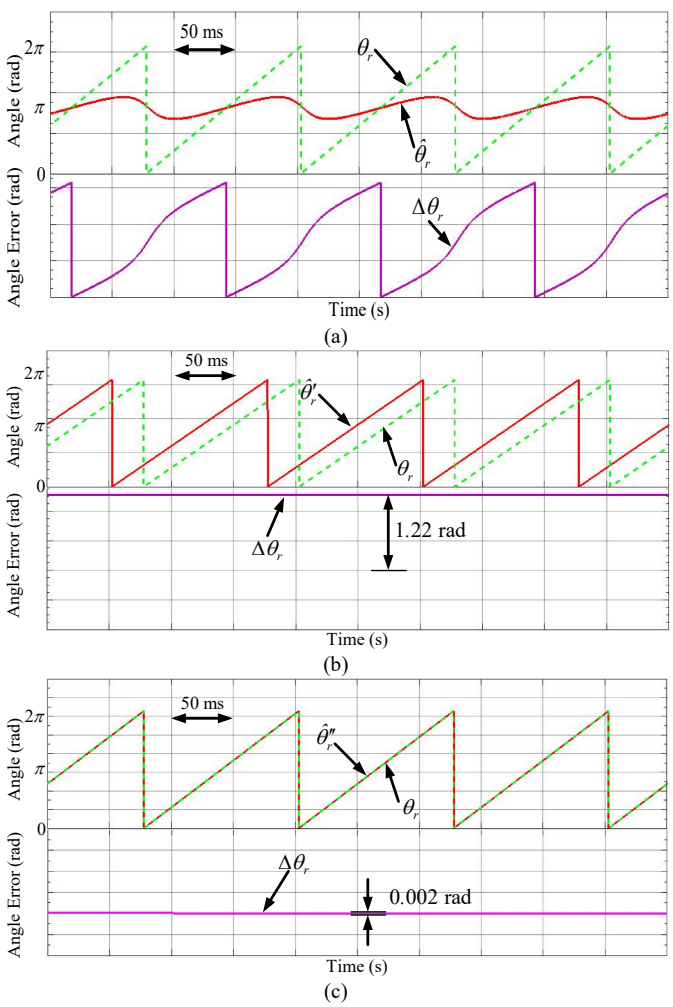

Fig. 7. Simulation results of the angle estimation at 200 r/min with no load. (a) Conventional flux observer, (b) IFO (before compensation), (c) IFO (after compensation).

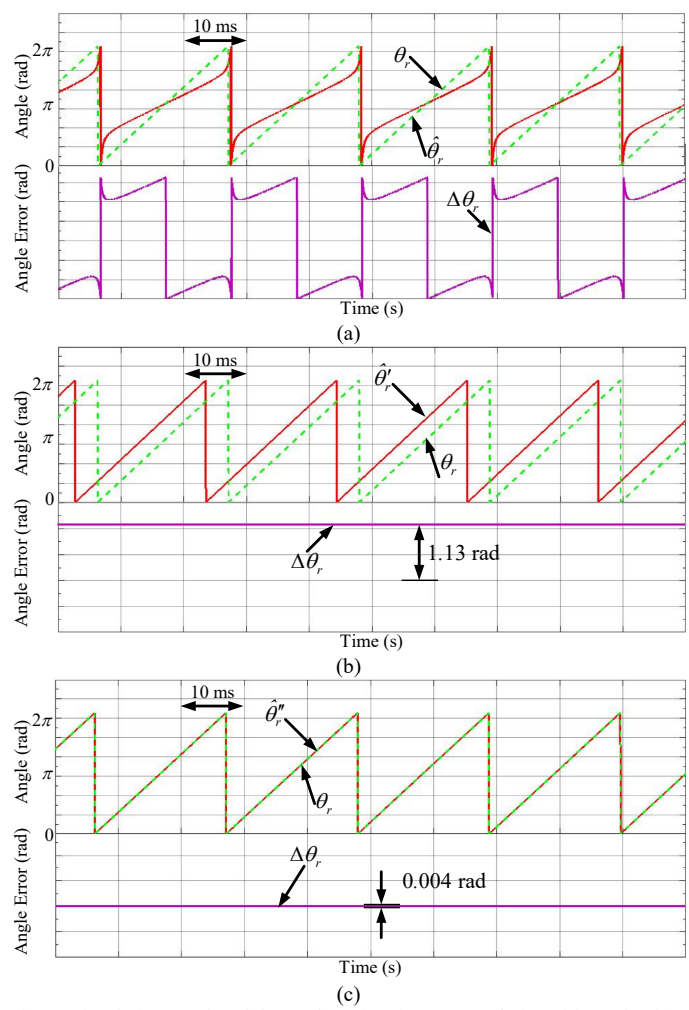

Fig. 8. Simulation results of the angle estimation at 900 r/min. with no load (a) Conventional flux observer, (b) IFO (before compensation), (c) IFO (after compensation).

compensation. But in order to ensure to accuracy of the estimated rotor position, it is necessary to compensate the estimated by the IPLL.

To further validate the parameter robustness of the IFO, the simulation results of parameter variation are shown in Fig. 9. Fig. 9 (a) shows the estimated angle error while stator resistance and *q-axis* stator inductance change with on ±50% of their nominal values. Fig. 9 (b) shows the estimated speed error when the stator resistance and *q-axis* stator inductance change with ±50% of their nominal values. As can be seen, the estimated angle error maintains at about 4 degrees when R_s and L_q change with ±50%. Simultaneously, the estimated speed error maintains about 0.4 r/min when parameters change. Therefore, parameter variation seldom exerts influence on the estimated rotor position, which demonstrate strong parameter robustness of the proposed method.

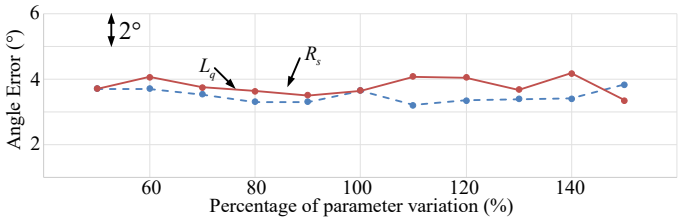

(a)

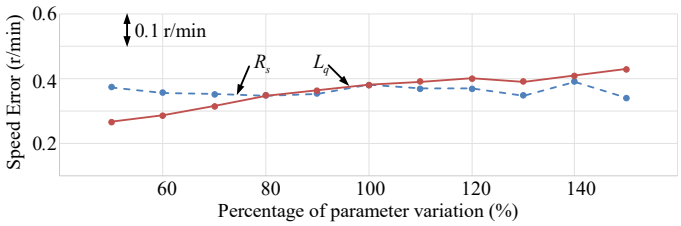

(b)

Fig. 9. Simulation results of parameter variation of R_s and L_q . (a) Estimated angle error, (b) Estimated speed error.

B. Experimental Results

To further demonstrate the effectiveness of IFO, the proposed sensorless control strategy is implemented in a PMSM drive system, controlled by a TI TMS 320F28335 DSP board. The platform of the PMSM drive system is shown in Fig. 10.

In this figure, an asynchronous induction machine (IM), which is connected with PMSM by a torque sensor is used as a load. The load can be changed by adjusting the current of the IM. Block diagram of drive system is shown in Fig. 11.

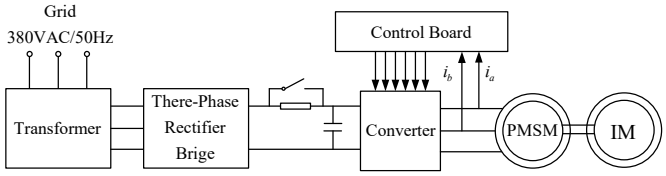

Fig.11. Block diagram of drive system.

In this system, dc voltage is supplied by the grid through transformer and three-phase Rectifier Bridge. The control board sends out three-phase pulse width modulation to the converter to control PMSM. In addition, the sampled currents

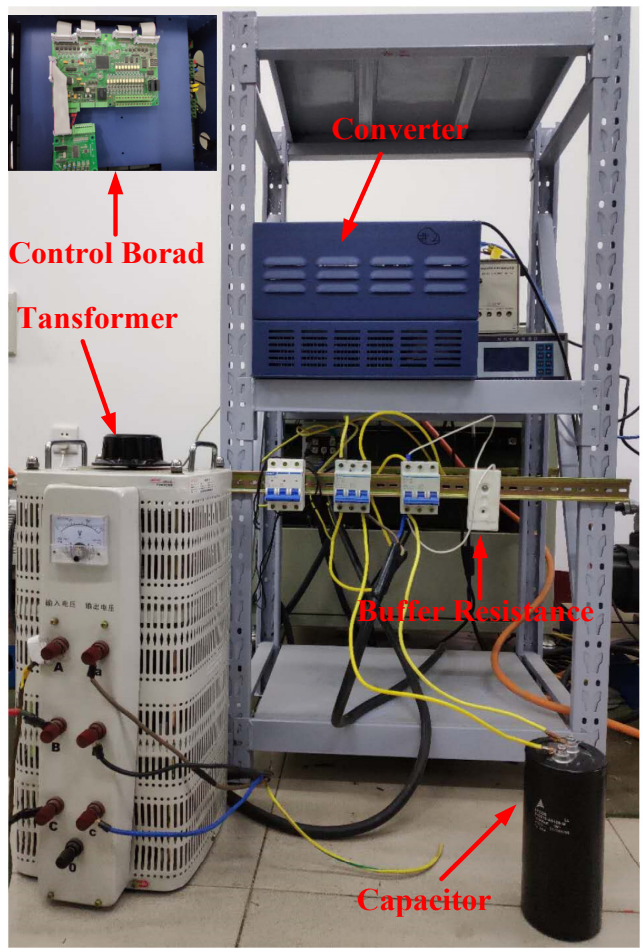

(a)

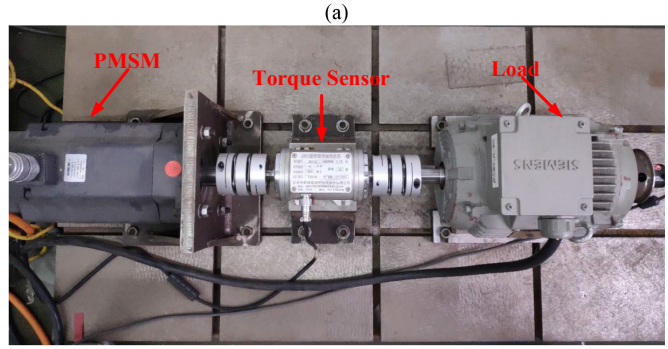

(b)

Fig.10. Platform of PMSM test drive system.

and voltages are sent to control board to obtain the estimated speed, estimated position and generate the PWM wave forms. The sampling frequency is 10 kHz.

Fig. 12 presents the experimental results of three methods at 200 r/min with no load. Fig. 12 (a) shows the estimated rotor position and position error of the conventional flux observer. It is obvious that the conventional flux observer is still unable to estimate the rotor position accurately in the experimental results. Fig. 12 (b) shows the estimated angle and angle error of the proposed IFO (before compensation). In this figure, the accuracy of rotor speed estimated by IFO regardless of phase compensation is demonstrated. However, due to the mismatch of the self-adaptive resonant angular frequency and estimated rotor angular frequency, there exist an angle error (about 3.4 rad) between estimated rotor position and actual rotor position.

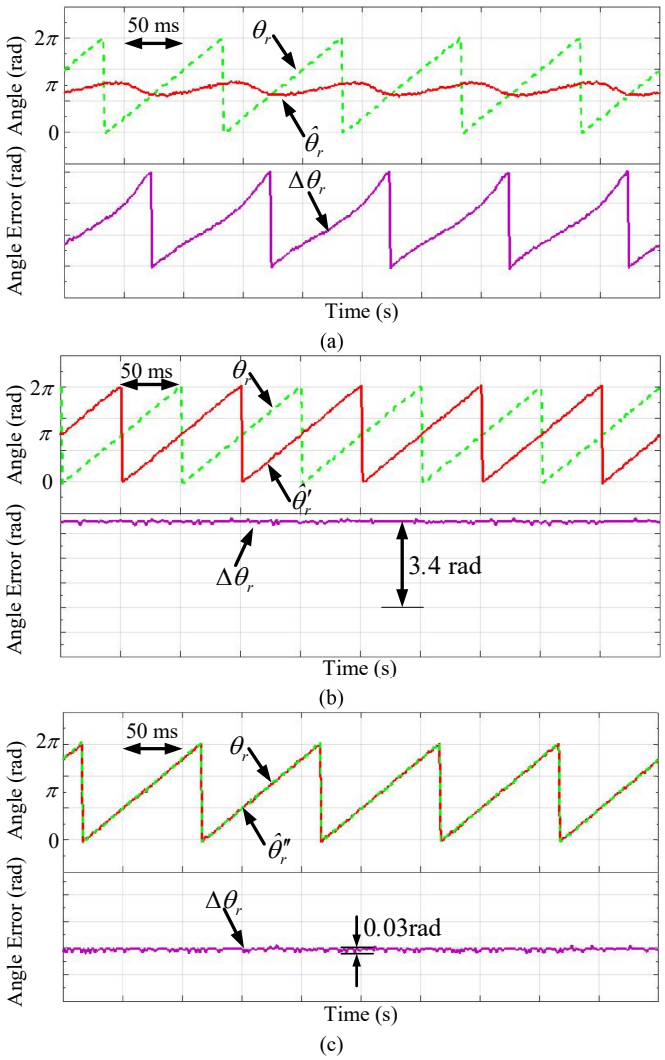

Fig.12. Experimental results of angle estimation at 200 r/min with no load. (a) Conventional flux observer, (b) IFO (before compensation), (c) IFO (after compensation).

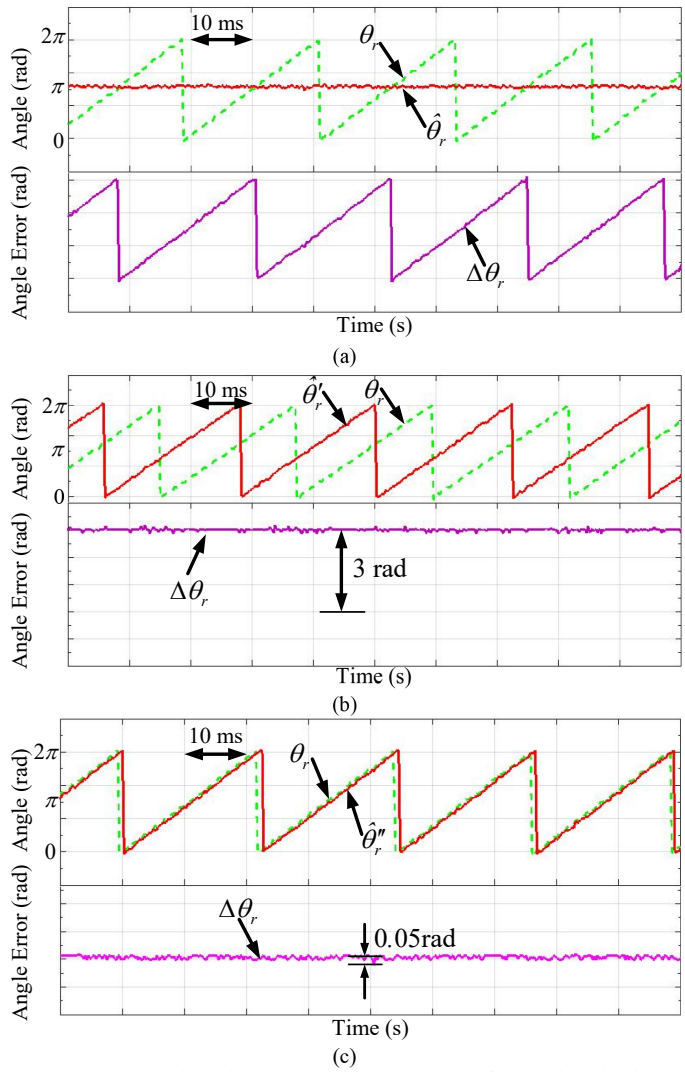

Fig.13. Experimental results of angle estimation at 900 r/min with no load. (a) Conventional flux observer, (b) IFO (before compensation), (c) IFO (after compensation).

Fig. 12 (c) presents the estimated rotor position and position error of IFO (after compensation). As it can be seen, the angle error is decreased to less than 0.05 rad after phase compensation. From Fig. 12 (b) and Fig. 12 (c) can be seen that the proposed method, IFO, is able to estimate the rotor speed and position accurately at low speed.

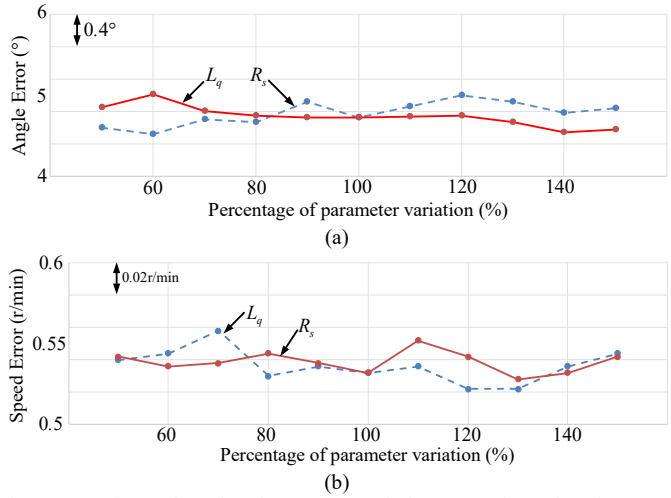

Fig.14. Experimental results of parameter variation. (a) Estimated angle error, (b) Estimated speed error.

Fig. 13 presents the simulation results of the three methods at 900 r/min with no load. Fig. 13 (a) shows the estimated rotor position and position error of the conventional flux observer. Fig. 13 (b) shows the estimated angle and angle error using the proposed IFO (before compensation). Fig. 13 (c) presents the estimated rotor position and position error of IFO (after compensation). As it can be seen, the conventional flux observer is still unable to estimate the rotor speed and position accurately. And the IFO can accurately obtain the rotor speed regardless of phase compensation. But in order to ensure an accuracy of the estimated rotor position, it is necessary to compensate the estimated by using the IPLL.

To further validate the parameter robustness of IFO, the experimental results of parameter variation are shown in Fig. 14. In this figure, the estimated angle error changes about 0.8 degree when R_s and L_q change with ±50% of their nominal values. Simultaneously, the estimated speed error changes about 0.04 r/min when parameters change. Therefore, the proposed method has a strong parameter robustness.

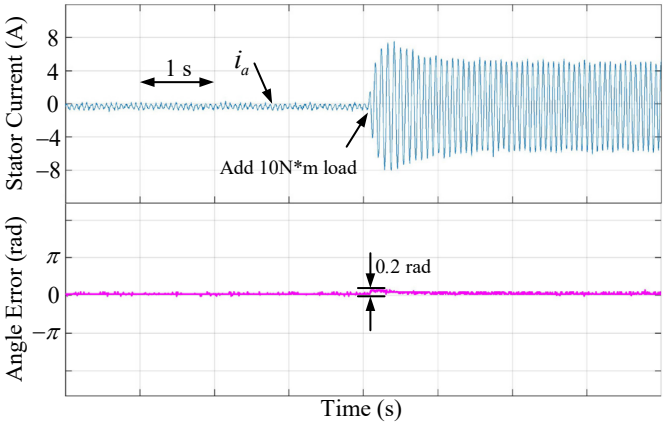

Fig.15. Experimental result of estimated error when load changes from 0 to 100% rated torque.

Fig.15 shows the experimental results of estimated error when load changes from 0 to 100% rated torque. It is obvious that the maximum estimated angle error is 0.2 rad when load changes from 0 to 100% rated torque. Therefore, the performance of IFO under the load changes is satisfactory.

V. Conclusion

In this paper, an improved flux observer method is proposed. To eliminate the angle error caused by current sampling and nonlinearity of converter, an SABPF is used to eliminate the DC component and high-frequency harmonics. In addition, an IPLL is designed to obtain the rotor speed. In order to avoid that the design of PI parameter is influenced by the amplitude of equivalent rotor flux linkage, the IPLL is employed to normalize the estimated equivalent rotor flux linkage. Furthermore, the phase shift is compensated, which is generated by the mismatch of self-adaptive resonant angular frequency and estimated rotor angular frequency. Several simulations and experiments are carried out on a 30 kW PMSM at lower and higher speed. Moreover, simulation and experiments when stator resistance and q-axis stator inductance change with ±50% of their nominal values are presented. All the simulation and experimental results prove the satisfactory performance and strong parameter robustness of the proposed method.

References

[1] M.A. Hoque, M.A. Rahaman, Speed and Position Sensorless Permanent Magnet Synchronous Motor Drives, *IEEE Anadien Conference on Electrical and Computer engineering*, CCECE, pp. 689-692, 1994.

[2] J. Liu, T. A. Nondahl, P. B. Schmidt, S. Royak and M. Harbaugh, "Rotor Position Estimation for Synchronous Machines Based on Equivalent EMF," *IEEE Trans. Ind. Appl*., vol. 47, no. 3, pp. 1310-1318, May-June 2011.

[3] X. Song, J. Fang, and B. Han, "Adaptive compensation method for high speed surface PMSM sensorless drives of EMF-based position estimation error," *IEEE Trans. Power Electron.*, vol. 31, no. 2, pp. 1438–1449, Feb. 2016.

[4] H. B. Azza, N. Zaidi, M. Jemli, and M. Boussak, "Development and Experimental Evaluation of a Sensorless Speed Control of SPIM Using Adaptive Sliding Mode-MRAS Strategy," *IEEE J. Emerg. Sel. Topics Power Electronics.*, vol. 2, no. 2, pp. 319-328, June 2014.

[5] V. Repecho, D. Biel and A. Arias, "Fixed Switching Period Discrete-Time Sliding Mode Current Control of a PMSM," *IEEE Trans on Industrial Electronics*, vol. 65, no. 3, pp. 2039-2048, March 2018.

[6] H. Kim, J. Son and J. Lee, "A High-Speed Sliding-Mode Observer for the Sensorless Speed Control of a PMSM," *IEEE Trans. Ind Electron.,* vol. 58, no. 9, pp. 4069-4077, Sept. 2011.

[7] S. Bolognani, R. Oboe and M. Zigliotto, "Sensorless full-digital PMSM drive with EKF estimation of speed and rotor position," *IEEE Trans. Ind. Electron.,* vol. 46, no. 1, pp. 184-191, Feb. 1999.

[8] G. Wang, Z. Li, G. Zhang, Y. Yu and D. Xu, "Quadrature PLL-Based High-Order Sliding-Mode Observer for IPMSM Sensorless Control With Online MTPA Control Strategy," *IEEE Trans. Energy Convers,* vol. 28, no. 1, pp. 214-224, March 2013.

[9] X. Zhang, H. Li, S. Yang and M. Ma, "Improved Initial Rotor Position Estimation for PMSM Drives Based on HF Pulsating Voltage Signal Injection," *IEEE Trans. Ind. Electron.*, vol. 65, no. 6, pp. 4702-4713, June 2018.

[10] X. Luo, Q. Tang, A. Shen and Q. Zhang, "PMSM Sensorless Control by Injecting HF Pulsating Carrier Signal Into Estimated Fixed-Frequency Rotating Reference Frame," *IEEE Trans. Ind. Electron.*, vol. 63, no. 4, pp. 2294-2303, April 2016.

[11] P. Rodriguez, A. Luna and I. Candela, "Multiresonant frequency-locked loop for grid synchronization of power converters under distorted grid conditions," *IEEE Trans. Ind. Electron*., vol. 58, no. 1, pp. 127-138, Jan. 2011.

[12] G. Feng, C. Lai, and K. Mukherjee, "Online PMSM magnet flux estimation for rotor magnet condition monitoring using harmonics in speed measurements," *IEEE Trans. Ind. Appl.*, vol. 53, no. 3, pp. 2786–2794, Feb. 2017.

[13] Y. Jiang, W. Xu and C. Mu, "Improved SOIFO-based rotor flux observer for PMSM sensorless control," *IECON 2017 - 43rd Annual Conference of the IEEE Industrial Electronics Society*, Beijing, 2017, pp. 8219-8224.

[14] W. Xu, Y. Jiang, C. Mu and F. Blaabjerg, "Improved Nonlinear Flux Observer-Based Second-Order SOIFO for PMSM Sensorless Control," *IEEE Trans. Power Electron.*, vol. 34, no. 1, pp. 565-579, Jan. 2019.

[15] Y. Liu, W. Xu, L. Ke and F. Blaabjerg, "An improved synchronous reference frame phase-locked loop for stand-alone variable speed constant frequency power generation systems," *2017 20th International Conference on Electrical Machines and Systems (ICEMS)*, Sydney, NSW, 2017, pp. 1-5.

Wei Xu (M'09-SM'13) received the double B.E. and M.E. degrees from Tianjin University, Tianjin, China, in 2002 and 2005, and the Ph.D. from the Institute of Electrical Engineering, Chinese Academy of Sciences, in 2008, respectively, all in electrical engineering.

From 2008 to 2012, he held several academic positions in both Australian and Japanese universities and companies. Since 2013, he has been full professor with the State Key Laboratory of Advanced Electromagnetic Engineering and Technology, Huazhong University of Science and Technology, China. His research topics mainly cover design and control of linear/rotary machines. He is Fellow of the Institute of Engineering and Technology (IET). He has served as Associate Editor for several Journals, such as IEEE Transactions on Industrial Electronics, IEEE Journal of Emerging and Selected Topics in Power Electronics, IEEE Transactions on Vehicular Technology, etc.

Lei Wang received the B.S. degree in electrical engineering from Huazhong University of Science and Technology, Wuhan, China, in 2013. He is currently working toward the M.S. degree in the School of Electrical and Electronic Engineering, Huazhong University of Science and Technology, Wuhan.

His research interests include advanced control methods for power electronics.

Yi Liu (M'14) received his B.E. and M.E. degrees in Automation and Control Engineering from the Wuhan University of Science and Technology, Wuhan, China, in 2004 and 2007, respectively; and his Ph.D. degree in Mechatronic Engineering from the Huazhong University of Science and Technology, Wuhan, China, in 2016.

From 2007 to 2011, he was a Lecturer at the City College, Wuhan University of Science and Technology, Wuhan, China. From March 2016 to June 2016, he was a Senior R&D Engineer at the Fourth Academy of China Aerospace Science and Industry Group, Wuhan, China. In July 2016, he became a Postdoctoral Research Fellow at the State Key Laboratory of Advanced Electromagnetic Engineering and Technology, School of Electrical and Electronic Engineering, Huazhong University of Science and Technology.

His current research interests include AC electrical machine control and inverter systems.

Frede Blaabjerg (S'86–M'88–SM'97–F'03) was with ABB-Scandia, Randers, Denmark, from 1987 to 1988. From 1988 to 1992, he got the PhD degree in Electrical Engineering at Aalborg University in 1995. He became an Assistant Professor in 1992, an Associate Professor in 1996, and a Full Professor of power electronics and drives in 1998. From 2017 he became a Villum Investigator.

His current research interests include power electronics and its applications such as in wind turbines, PV systems, reliability, harmonics and adjustable speed drives. He has published more than 500 journal papers in the fields of power electronics and its applications. He is the co-author of two monographs and editor of 7 books in power electronics and its applications.

He has received 24 IEEE Prize Paper Awards, the IEEE PELS Distinguished Service Award in 2009, the EPE-PEMC Council Award in 2010, the IEEE William E. Newell Power Electronics Award 2014 and the Villum Kann Rasmussen Research Award 2014. He was the Editor-in-Chief of the IEEE TRANSACTIONS ON POWER ELECTRONICS from 2006 to 2012. He has been Distinguished Lecturer for the IEEE Power Electronics Society from 2005 to 2007 and for the IEEE Industry Applications Society from 2010 to 2011 as well as 2017 to 2018. In 2018 he is President Elect of IEEE Power Electronics Society.

He is nominated in 2014, 2015, 2016 and 2017 by Thomson Reuters to be between the most 250 cited researchers in Engineering in the world. In 2017 he became Honoris Causa at University Politehnica Timisoara (UPT), Romania.